RESEARCHERID
THOMSON REUTERS

[Mishra* *et al.*, 6(4): April, 2017]
IC™ Value: 3.00

ISSN: 2277-9655
Impact Factor: 4.116
CODEN: IJESS7

IJESRT

INTERNATIONAL JOURNAL OF ENGINEERING SCIENCES & RESEARCH TECHNOLOGY

SLIP EFFECT ON MHD FLOW AND HEAT TRANSFER OF JEFFREY NANOFLUID OVER A STRETCHING SHEET IN THE PRESENCE OF NONLINEAR THERMAL RADIATION AND CHEMICAL REACTION

Raghawendra Mishra*
* Department of Mathematics, Government P.G. College. Ranikhet

DOI: 10.5281/zenodo.557138

ABSTRACT

Analysis has been conducted to analyze the effects of second order slip flow and heat transfer of Jeffrey nanofluid over a stretching sheet with non linear thermal radiation and chemical reaction. The effects of Brownian motion and thermophoresis occur in the transport equations. The velocity, temperature and nanoparticle concentration profiles are analyzed with respect to the involved parameters of interest namely Brownian motion parameters, thermophoresis parameter, magnetic parameter, radiation parameter, Prandtl number, Lewis number, chemical reaction parameter, and Deborah number, Convergence of the derived solutions was checked and the influence of embedded parameters was analyzed by plotting graphs. It was noticed that the velocity increases with an increase in the Deborah number. We further found that for fixed values of other parameters, numerical values of the skin friction coefficient, local Nusselt numbers and Sherwood numbers were computed and examined. A comparative study between the previous published and present results in a limiting sense is found in an excellent agreement.

KEYWORDS: Jeffrey fluid, nonlinear thermal radiation, chemical reaction, second order slip, numerical solution.

INTRODUCTION

The boundary layer flow analysis of an electrically conducting fluid due to a stretching sheet is of great interest because of their diverse engineering and industrial applications.MHD has immediate applications in designing of heat exchangers, in space vehicle propulsion, in thermal protection, in agnetohydrodynamic (MHD) power generators, MHD pumps, in polymer technology, in petroleum industry, in purification of crude oil and fluid droplets sprays. Its relevance is also seen in the fields of stellar and planetary magnetospheres, aeronautics, chemical engineering and electronics. In this view, many authors [1–6] have recently studied the MHD effects on flow problems with different aspects. They found that, MHD effect have a significant role in thermal management applications.

In the recent years, micro-scale fluid dynamics in the Micro-Electro-Mechanical Systems (MEMS) received much attention in research. Because of the micro-scale dimensions, the fluid flow behavior belongs to the slip flow regime and greatly differs from the traditional flow [7]. For the flow in the slip regime, the fluid motion still obeys the Navier–Stokes equations, but with slip velocity or temperature boundary conditions. In addition, partial velocity slips over a moving surface occur for fluids with particulate such as emulsions, suspensions, foams, and polymer solutions [8]. The slip flows under different flow configurations have been studied in the literature [9–14]. Hayat et al. [15] studied the steady three-dimensional boundary layer flow of water based nanofluid with copper as nanoparticle over a permeable stretching surface with second order velocity slip and homogeneous–heterogeneous reactions. Zhu et al. [16] are investigated the effects of the second-order velocity slip and temperature jump boundary conditions on the magnetohydrodynamic (MHD) flow and heat transfer of water-based nanofluids containing Cu and Al_2O_3 in presence of thermal radiation. Megahed [17] obtained numerical solution to study the boundary layer flow and heat transfer for an electrically conducting Casson fluid over a permeable stretching surface with second-order slip velocity model and thermal slip conditions in the presence of internal heat generation/absorption and thermal radiation and he shown that increasing the velocity and thermal slip parameters makes the rate of heat transfer decrease. Hakeem et al. [18] performed both numerical and analytical analysis to study the effect of magnetic field on a steady two dimensional laminar radiative flow of an incompressible viscous water based nanofluid over a stretching/shrinking sheet with second order slip boundary condition.

Besides, the radiative heat transfer have wide occurrence in various applications, such as in nuclear power plants, gas turbines, propulsion devices for space vehicles, missiles and aircraft etc. In view of these applications, many researchers [19–23] have considered the influence of thermal radiation effect with different physical situations. To simplify the radiative heat flux the Rosseland approximation has been employed. Further, they have assumed small temperature differences within the flow to make out the linear radiative heat flux. But in recent years, many authors have an interest in the study of non-linear thermal radiation effect (see [24–27]).

It is now a well-accepted fact that many fluids of industrial and geophysical importance are non-Newtonian. Due to much attention in many industrial applications, such as the extrusion of plastic sheets, fabrication of adhesive tapes, glass-fiber production, metal spinning, and drawing of paper films. Recently, some research has been focused on the study of nanofluids. Nanofluids are a homogenous mixture of a base fluid and nanoparticles. The term nanofluid was first introduced by Choi [28] to describe engineered colloids composed of nanoparticles dispersed in a base fluid. Many studies are focused on non-Newtonian fluid as a base fluid with suspended nanoparticles over a stretching sheet [29, 30, 31] Hayat et al. [32] studied the effects of thermophoresis and Brownian motion on the three-dimensional (3D) boundary layer flow and convective heat transfer of Jeffrey nanofluid over a bidirectional stretching surface with newly developed boundary condition with the zero nanoparticles mass flux. Shehzad et al. [33, 34] investigated the effects of convective heat and concentration conditions in magnetohydrodynamic two-dimensional and three-dimensional flow of Jeffrey nanofluid fluid with nanoparticles. Dalira et al. [35] numerically studied the entropy generation for steady laminar two-dimensional forced convection magnetohydrodynamic (MHD) boundary layer flow, heat transfer and mass transfer of an incompressible non-Newtonian nanofluid over a linearly stretching, impermeable and isothermal sheet with viscous dissipation. Recently, Prasannakumara et al [36] studied the Effects of chemical reaction and nonlinear thermal radiation on Williamson nanofluid slip flow over a stretching sheet embedded in a porous medium.

The purpose of present paper is to analyze the effect of second order slip and nonlinear thermal radiation on heat and momentum transfer of steady two-dimensional slip flow of a nanofluid over a stretching sheet. Reduced governing nonlinear ordinary differential equations are solved numerically by means of Runge-Kutta-Fehlberg-45 order method. The effects of different flow parameters on flow fields are elucidated through graphs and tables.

MATHEMATICAL FORMULATION

Let us consider a steady flow of an incompressible Jeffrey nanofluid over a horizontal stretching surface. The flow region is confined to $y > 0$ and the plate is stretched along x-axis with a velocity $U_w = ax$, where a is a positive constant. A uniform magnetic field B_0 is applied in the transverse direction y normal to the plate. The nanofluid is assumed to be single phase, in thermal equilibrium and there is a slip velocity between the base fluid and particles. The stretching surface temperature and the nanoparticles fraction are deemed to have constant value T_w and C_w, respectively. The ambient fluid temperature and nanoparticales fraction have constant value T_∞ and C_∞, respectively. The coordinate system and flow regime is illustrated as shown in the figure 1.

It is well known that the constitutive equations for a Jeffrey fluid are given by (2015)

$$\tau = -pI + S,$$
$$S = \frac{\mu}{1+\lambda}\left[R_1 + \lambda_1\left(\frac{\partial R_1}{\partial t} + V.\nabla\right)R_1\right],$$

whereτ is the Cauchy stress tensor, S is the extra stress tensor, μ is the dynamic viscosity, λ and λ_1 are the material parameters of Jeffrey fluid and R_1 is the Rivlin–Ericksen tensor defined by

$$R_1 = (\nabla V) + (\nabla V)'.$$

Under usual boundary layer approximations governing two-dimensional equations for the present problem are given as follows (2009):

$$\frac{\partial u}{\partial x} + \frac{\partial v}{\partial y} = 0, \tag{2.1}$$

$$u\frac{\partial u}{\partial x} + v\frac{\partial u}{\partial y} = \frac{\nu}{1+\lambda}\left[\frac{\partial^2 u}{\partial y^2} + \lambda_1\left(u\frac{\partial^3 u}{\partial x \partial y^2} + v\frac{\partial^3 u}{\partial y^3} - \frac{\partial u}{\partial x}\frac{\partial^2 u}{\partial y^2} + \frac{\partial u}{\partial y}\frac{\partial^2 u}{\partial x \partial y}\right)\right] - \frac{\sigma {B_0}^2}{\rho_f}u, \tag{2.2}$$

$$u\frac{\partial T}{\partial x}+v\frac{\partial T}{\partial y}=\alpha\frac{\partial^2 T}{\partial y^2}+\frac{\rho_p c_p}{(\rho c)_f}\left[D_B\frac{\partial C}{\partial y}\frac{\partial T}{\partial y}+\frac{D_T}{D_\infty}\left(\frac{\partial T}{\partial y}\right)^2\right]-\frac{1}{(\rho c)_f}\frac{\partial q_r}{\partial y}, \quad (2.3)$$

$$u\frac{\partial C}{\partial x}+v\frac{\partial C}{\partial y}=D_B\frac{\partial^2 C}{\partial y^2}+\frac{D_T}{D_\infty}\frac{\partial^2 T}{\partial y^2}-k_1(C-C_\infty), \quad (2.4)$$

The corresponding boundary conditions are given by,

$$u=U_w+U_{slip},\ v=0,\ T=T_w,\ C=C_w\ at\ y=0,$$
$$u=0,\ T=T_\infty,\ \ C=C_\infty,\ \ as\ y\to\infty. \quad (2.5)$$

Where U_{slip} is the slip velocity at the surface and it is negative due to stretching. Wu's (2008) slip velocity model used in this paper is valid for arbitrary Knudsen numbers and is given as follows:

$$U_{slip}=\frac{2}{3}\left(\frac{3-\chi l^3}{\chi}-\frac{3}{2}\frac{1-l^2}{K_n}\right)\omega\frac{\partial u}{\partial y}=\frac{1}{4}\left[l^4+\frac{2}{K^2{}_n}(1-l^2)\right]\omega^2\frac{\partial^2 u}{\partial y^2}=A\frac{\partial u}{\partial y}+B\frac{\partial^2 u}{\partial y^2}, \quad (2.6)$$

where $l=\min[\frac{1}{k_N},1]$, χ is the momentum accommodation coefficient with $0\le\chi\le 1$, ω is the molecular mean free path, and K_n is the Knudsen number defined as the mean free path ω divided by a characteristic length for the flow. Based on the definition of l, it is seen that for any given value of K_n, we have $0\le l\le 1$. The molecular mean free path is always positive. Thus we know that $B<0$ and A is a positive number.

$A_1$is the first-order velocity slip parameter with $0<A_1=A\sqrt{\frac{a}{\nu}}$ and A_2 is the second-order velocity slip parameter with $0>A_2=\frac{Ba}{\nu}$.

Unlike the linearized Rosseland approximation, we use nonlinear Rosseland diffusion approximation from which one can obtainresults for both small and large differences between T_w and T_∞. Using Rosseland (Rosseland, 1931) approximation for radiation, the radiative heat flux is simplified as,

$$q_r=-\frac{4\sigma^*}{3k^*}\frac{\partial T^4}{\partial y}, \quad (2.7)$$

For a boundarylayer flow over a horizontal flat plate (Pantokratoras and Fang, 2013), from Eq. (2.7) we get,

$$q_r=\left(-\frac{16\sigma^* T_\infty{}^3}{3k^*}\right)\frac{dT}{dy}, \quad (2.8)$$

In view to Eq. (2.8),energy equation(2.3) takes the form

$$u\frac{\partial T}{\partial x}+v\frac{\partial T}{\partial y}=\frac{\partial}{\partial y}\left[\left(\alpha+\frac{16\sigma^* T_\infty{}^3}{3k^*(\rho c)_f}\right)\frac{\partial T}{\partial y}\right]+\frac{\rho_p c_p}{(\rho c)_f}\left[D_B\frac{\partial C}{\partial y}\frac{\partial T}{\partial y}+\frac{D_T}{D_\infty}\left(\frac{\partial T}{\partial y}\right)^2\right], \quad (2.9)$$

where $\alpha=\frac{k}{(\rho c)_f}$, k being the thermal conductivity.

The governing equations can be reduced to ordinary differential equations, using the following similarity transformations,

$$u=axf'(\eta),\quad v=-\sqrt{a\nu}f(\eta),\quad \eta=\sqrt{\frac{a}{\nu}}y,$$
$$T=T_\infty\big(1+(\theta_w-1)\theta(\eta)\big),\quad \phi(\eta)=\frac{C-C_\infty}{C_w-C_\infty}. \quad (2.10)$$

Where $\theta_w=\frac{T_w}{T_\infty}$, $\theta_w>1$ the temperature ratio parameter (Shehzad et al. 2014).

With the help of aforementioned transformations, equation (2.1) is identically satisfied and equations (2.2), (2.4) and (2.9) will take the following forms;

$$f'''+(1+\lambda)[ff''-f'^2]+\beta[f''^2-ff'''']-(1+\lambda)(M)f'=0, \quad (2.11)$$

$$[1+Nr\,(1+(\theta_w-1)\theta)^3\theta']'+\Pr[f\theta'+Nb\phi'\theta'+Nt(\theta')^2]=0, \quad (2.12)$$
$$\phi''+Lef\phi'+\frac{Nt}{Nb}\theta''-\gamma\phi=0, \quad (2.13)$$

The corresponding boundary conditions are;

$$f(0)=0,\ f'(0)=1+A_1 f''(0)+A_2 f'''(0),\ \theta(0)=1,\ \phi(0)=1 \ \text{ at } \eta=0,$$
$$f'(\eta)=\ f''(\eta)=\theta(\eta)=\phi(\eta)=0 \text{ as } \eta\to 0, \qquad (2.14)$$

where f, θ and ϕ are functions of η and prime denotes derivatives with respect to η. $\beta=a\lambda_1$ is Deborah number, $M=\frac{\sigma {B_0}^2}{\rho_f a}$ is magnetic parameter called Hartmann number, $Nr=\frac{16\sigma^* T^3{}_\infty}{3kk^*}$ is radiation parameter, $Nb=\frac{\tau D_B(C_w-C_\infty)}{\nu}$ is Brownian motion parameter, $Nt=\frac{\tau D_T(T_w-T_\infty)}{\nu T_\infty}$ is thermophoresis parameter, $Pr=\frac{\nu}{\alpha}$ is Prandtl number, $\gamma=\frac{k_1 Le}{a}$ is chemical reaction parameter, and $Le=\frac{\nu}{D_B}$ is Lewis number,

The skin friction coefficient (Cf_x), local Nusselt number (Nu_x) and Local Sherwood number (Sh_x) are given by,

$$Cf_x=\frac{\tau_w}{\rho U_w^2},\ \ Nu_x=\frac{xq_w}{k(T_w-T_\infty)} \text{ and } Sh_x=\frac{xq_m}{k(C_w-C_\infty)}, \qquad (2.15)$$

where the shear stress along the stretching surface τ_w, the surface heat flux q_w and the surface mass flux q_m are

$$\tau_w=\frac{\mu}{1+\lambda}\left[\left(\frac{\partial u}{\partial y}\right)+\lambda_1\left(\frac{\partial^2 u}{\partial x\partial y}+u\frac{\partial^2 v}{\partial x^2}+v\frac{\partial^2 u}{\partial y^2}\right)\right]_{y=0},$$
$$q_w=-k\frac{\partial T}{\partial y}+(q_r)_w,\ q_m=-D_B\frac{\partial C}{\partial y} \text{ at } y=0. \qquad (2.16)$$

Substituting the values of τ_w q_w and q_m into the equation (2.16) we have

$$\sqrt{Re}Cf_x=\left[\frac{1}{1+\lambda}\left(f''(0)+\beta\big(f'(0)f''(0)\big)-f(0)f'''(0)\right)\right],$$
$$\frac{Nu_x}{\sqrt{Re_x}}=-(1+Nr\theta^3{}_w)\theta'(0),\ \frac{Sh_x}{\sqrt{Re_x}}=-\phi'(0), \qquad (2.17)$$

where $Re_x=\frac{ax^2}{\nu}$ is local Reynolds number.

NUMERICAL METHOD

The system of non-linear ordinary differential equations (2.11) to (2.13) with boundary conditions (2.14) have been solved using Runge-Kutta-Fehlberg fourth-fifth order method along with Shooting technique. The method has the following steps: In the first step, the governing system of Eqs. (2.11) to (2.13) are reduced to a system of eight simultaneous differential equations of first order by introducing new dependent variables. In this system of first order differential equations, four initial conditions are known and remaining missed initial conditions are obtained with the help shooting technique. Afterward, a finite value for η_∞ is chosen in a such a way that all the far field boundary conditions are satisfied asymptotically. Our bulk computations are considered with the value at η_∞= 5, which is sufficient to achieve the far field boundary conditions asymptotically for all values of the parameters considered. After fixing finite value for η_∞, integration is carried out with the help of Runge-Kutta-Fehlberg-45(RKF-45) method. Runge-Kutta-Fehlberg-45 method has a procedure to determine if the proper step size h is being used. Ateach step, two different approximations for the solution are made and compared. If the two answers are in close agreement, the approximation is accepted otherwise, the step size is reduced until to get the required accuracy. For the present problem, we took step size $\Delta\eta=0.001, \eta_\infty=5$ and accuracy to the fifth decimal places. To have a check on the accuracy of the numerical procedure used, first test computations for $\theta'(0)$ are carried out for viscous fluid for various values of Pr and compared with the available published results of Goyal and Bhargava (2014), Gorla and Sidawi (1994), Nadeem and Hussain (2013) and Wang (1989) in table 1 and they are found to be in excellent agreement.

RESULTS AND DISCUSSION

A theoretical investigation of Second order velocity slip boundary layer flow of Jeffrey nanofluid over a stretching sheet under the influence of nonlinear thermal radiation and chemical reaction has been performed. The value of the Prandtl number for the base fluid is kept as $Pr=10$. The default values of the other parameters are mentioned in the description of the respected figures. In order to study the characteristics of velocity and temperature distribution for first ordervelocity slip parameter (A_1) and second order velocity slip parameter (A_2), Radiation parameter (Nr), temperature ratio parameter (θ_w), magnetic parameter (M) graphs are platted and physical reasons behind the trend of the graphs are discussed.

Effect of first order and second order velocity slip parameters on velocity and temperature profiles are demonstrated in Fig.2 and 3. We can observe that the effects of increasing values of both first and second order velocity slip parameters are reduces the thickness of momentum boundary layer and hence decrease the velocity. Therefore, increasing values of velocity slip coefficients (A_1 and A_2)decrease the boundary layer velocity, where

ISSN: 2277-9655
Impact Factor: 4.116
CODEN: IJESS7

as the temperature increase with increase in$A_1$and A_2. This must be due to the existence of slip velocity on the stretching surface.

Fig.4 describe the effects of Deborah number β on the velocity and temperature profiles. We can see thatboundary layer thickness and the fluid velocity increases with increase in β. It is because, increase in β decreases the resistance of fluid motionwhich thuscauses ahigher fluid movement at the neighborhood of the stretching surface. Fig.4 also reveals that larger values of Deborah number leads to a reduction in the temperature andthermal boundary layer thickness. It is due to the fact that Deborah number is directly proportional to relaxation time and larger values of Deborah number corresponds to the higher relaxation time. Such increase in relaxation time corresponds to the lower temperature andweaker thermal boundary layer thickness. We can also see that boost in β causes the reduction in the concentration boundary layer.

Influence of λ on velocity and temperature profile is highlighted in Fig.5. It can be seen that increase in λ decreases the fluid velocity but enhances temperature profile and it gives rise to the nanoparticle concentration field and associated boundary layer thickness. It is due to the fact that increase of λ corresponds to a decrease in retardation time but increase in the relaxation time and hence higher values of λ imply the domination of relaxation time over retardation time due to which temperature concentration profile are enhanced.

Fig.6 shows the effect of magnetic parameter M on dimensionless velocity and temperature distributions, respectively. The presence of a magnetic field in an electrically conducting fluid induces a force called Lorentz force, which opposes the flow. This resistive force tends to slow down the flow, so the effect of M decreases the velocity and also cause increase in its temperature distributions.

Figs.7 and 8 illustrates the effect of temperature ratio parameter θ_w on temperature profiles, when $Pr = 6.2$ and $Pr = 10$ respectively. From these plots, one can notice that, the increase in temperature ratio parameter increases the thermal state of the fluid, and it results in increase of temperature profiles. The effect of radiation parameter on temperature is depicted as in Fig.9. A critical observation shows that, the temperature profile increases with increase in Nr. This is because, an increase in the radiation parameter provides more heat to fluid that causes an enhancement in the temperature and thermal boundary layer thickness.

Effect of chemical reaction parameter γ on nanoparticle volume fraction profile is shown in Fig.10 for the several values of $\gamma(> 0)$ and $\gamma(< 0)$ cases. It is observed that the nanoparticles volume fraction decreases for constructive chemical reaction parameter and increases for destructive chemical reaction parameter.

Figs.11 and 12 displays the effect of Lewis number Le on temperature and concentration profiles. From these figures both the profiles decreases with increasing the values of the Le. It is due to the fact that the larger values of Lewis number makes the mass diffusivity smaller, therefore it decreases the concentration field.

Temperature and nanoparticles volume fraction variation against different values of Nb and Nt are depicted respectively, as in Figs. 13 to 15. We can see that the temperature profiles are increasing function of Nb, whereas nanoparticles volume fraction is a decreasing. This may be due to the fact that as a Brownian motion parameter Nb decreases the mass transfer of a nanofluid. Further both temperature and nanoparticles volume fraction profiles increases for increasing values of Nt. The variation in Prandtl number Pron θ is shown in Fig.16. The temperature field θ decreases when Pr increases. It is obvious that an increase in the values of Pr reduces the thermal diffusivity therefore thermal boundary layer thickness is decreasing function of Pr.

The numerical results are recorded in table 2, and it illustrates the variation of skin friction co-efficient and Nusselt number with respect to various flow controlling parameters.As expected, both first order and second order velocity slip parameters effect is to reduce the friction at the solid-fluid interface, and thus reduces the skin friction coefficient. Similar behaviour is also observed in the case of λ, i.e in the presence velocity slip, increase inλ results decrease of both skin friction coefficient and local Nusselt number. But quite opposite behaviour is observed in case of β and M

The effects of various pertinent parameters on local Nusselt number and local Sherwood number is discussed numerically through table 3. We can see that γ, Le and Pr shows favourable effect on coefficient of $\phi'(0)$, whereas effect of θ_w, Nb and Nt on local Nusselt number is negligible. We can also observe that both θ_w and

ISSN: 2277-9655
Impact Factor: 4.116
CODEN: IJESS7

Pr show positive effect on local Nusselt number. This is due to the fact that a higher Prandtl number reduces the thermal boundary layer thickness and increases the surface heat transfer rate. Also high Prandtl number implies more viscous fluid which tends to retard the motion. Similarly and θ_w shows negative effect and chemical parameter has no effect on local Nusselt number.

CONCLUSION

A boundary layer analysis to study the effect of nonlinear thermal radiation on Second order Slip flow and heat transfer of Jeffrey nanofluid over a stretching sheet with chemical reaction is presented. Numerical results for velocity profiles, surface heat transfer rate and mass transfer rate have been obtained for parametric variations of various ranges of slip boundary condition and for different values of flow pertinent parameters. The main outcomes of the problem are summarized as follow;

- Both first and second order velocity slip parameters are reduces the thickness of momentum boundary layer and hence decrease the velocity.
- Boundary layer thickness and the fluid velocity increases with increase in Deborah number .
- An increase in Lewis and Prandtl numbers shows a decrease in nanoparticles concentration.
- Larger values of magnetic parameter M lead to an enhancement in the temperature and nanoparticles concentration.
- Increase in λ and $\theta_w$enhances thetemperature profile.
- Nanoparticles volume fraction decreases for constructive chemical reaction parameter and increases for destructive chemical reaction parameter.
- Both temperature and nanoparticles volume fraction increase for increasing values of Nr.
- Nrenhances coefficient of Nusselt number, but the parametersθ_w, Nb, Nt decreases $-\theta'(0)$.

NOMENECLAURE

u, v	velocity components along the x and y axes
k^*	Rosseland mean absorption coefficient
D_B	Brownian diffusion coefficient
D_T	thermophoresis diffusion coefficient
B_0	magnetic field strength
Cf_x	local skin friction coefficient
Nu_x	localNusselt number
Sh_x	local Sherwood number
k_1	chemical reaction coefficient
A_1	is the first-order velocity slip parameter
A_2	is the second-order velocity slip parameter
C	volumetric volume expansion coefficient
T	temperature of the nanofluid near wall
T_∞	fluid temperature far away from the sheet
T_w	uniform wall temperature
k	thermal conductivity
U_w	stretching velocity
a	stretching rate
M	magnetic parameter

Re_x	local Reynolds number
Pr	Prandtl number
Nr	radiation parameter
Le	Lewis number
Nb	Brownian motion parameter
Nt	thermophoresis parameter.
Greek symbols	
λ, λ_1	ratio of relaxation and retardation times and the relaxation time
ρ_f	density of the fluid
ρ_p	nanoparticles density
θ	dimensionless temperature variable
ϕ	nanoparticles volume fraction
α	thermal diffusivity
η	similarity variable
ν	kinematic viscosity
σ^*	Stefan-Boltzmann constant
$(\rho c)_f$	heat capacities of nanofluid
$(\rho c)_p$	effective heat capacity of the nanoparticles
β	Deborah number
γ	chemical reaction parameter
Subscripts	
∞	infinity
w	sheet surface

REFERENCES

[1] Hayat T, Mehmood OU. Slip effects on MHD flow of third order fluid in planar channel. Commun Nonlinear Sci Numer Simul 2013;16(3): 1363–77.
[2] Nadeem S, Hussain M, Naz M. MHD stagnation flow of a micropolar fluid through a porous medium. Int J Meccanica 2010;45:869–80.
[3] KJha B, Apere CA. Unsteady MHD two phase Couette flow of fluid-particle suspension. Appl Math Model 2013;37:1920–31.
[4] Makinde OD, Chinyoka T. MHD transient flow and heta trabnsfer of dusty fluid in channel with variable physical parameters and Navier slip boundary condition. Comput Math Appl 2010;60:660–9.
[5] Gireesha BJ, Mahanthesh B, Rashidi MM. MHD boundary layer heat and mass transfer of a chemically reacting Casson fluid over a permeable stretching surface with non-uniform heat source/sink. Int J Ind Math 2015;7:14.
[6] Gireesha BJ, Mahanthesh B, Manjunatha PT, Gorla RSR. Numerical solution for hydromagnetic boundary layer flow and heat transfer past a stretching surface embedded in non-Darcy porous medium with fluid-particle suspension. J Nigerian Math Soc 2015;34(3):267–85.
[7] Gal-el-Hak M. The fluid mechanics of microdevices – The Freeman Scholar Lecture. J Fluids Eng Trans ASME 1999;121:5–33.
[8] Yoshimura A, Prudhomme RK. Wall slip corrections for Couette and parallel disc viscometers. J Rheol 1988;32:53–67.
[9] Andersson HI. Slip flow past a stretching surface. Acta Mech 2002;158:121–5.
[10] Wang CY. Flow due to a stretching boundary with partial slip – an exact solution of the Navier–Stokes equations. Chem Eng Sci 2002;57(17):3745–7.
[11] Fang T, Lee CF. Exact solutions of incompressible Couette flow with porous walls for slightly rarefied gases. Heat Mass Transfer 2006;42(3):255–62.
[12] Wang CY. Stagnation slip flow and heat transfer on a moving plate. Chem Eng Sci 2006;61(23):7668–72.
[13] Wang CY. Stagnation flow on a cylinder with partial slip – an exact solution of the Navier–Stokes equations. IMA J Appl Math 2007;72(3):271–7.
[14] Wang CY. Analysis of viscous flow due to a stretching sheet with surface slip and suction. Nonlinear Anal Real World Appl 2009;10(1):375–80.
[15] Hayat, T., Taseer Muhammad, Alsaedi, A and Alhuthali, M.S. Magnetohydrodynamic three-dimensional flow of viscoelastic nanofluid in the presence of nonlinear thermal radiation. Journal of Magnetism and Magnetic Materials, 2015;385: 222–229.
[16] Jing Zhu, Liu Zheng, Liancun Zheng and Xinxin Zhang. Second-order slip MHD flow and heat transfer of nanofluids with thermal radiation and chemical reaction. Applied Mathematics and Mechanics ,2015 ; 36(9):1131-1146.
[17] Megahed, A. M. MHD viscous Casson fluid flow and heat transfer with second-order slip velocity and thermal slip over a permeable stretching sheet in the presence of internal heat eneration/absorption and thermal radiation. The European Physical Journal Plus, 2015; 130: 81.
[18] Abdul Hakeem, A.K., Vishnu Ganesh, N and Ganga, B. Magnetic field effect on second order slip flow of nanofluid over a stretching/shrinking sheet with thermal radiation effect. Journal of Magnetism and Magnetic Materials 2015; 381: 243–257.
[19] Pop SR, Grosan T, Pop I. Radiation effects on the flow near the stagnation point of a stretching sheet. Tech Mech 2004;25(2):100–6.
[20] Akbar NS, Nadeem S, Ul Haq R, Khan ZH. Radiation effects on MHD stagnation point flow of nano fluid towards a stretching surface with convective boundary condition. Chin J Aeronaut 2013;26:1389–97.
[21] Cortell R. Effects of viscous dissipation and radiation on the thermal boundary layer over a non-linearly stretching sheet. Phys Lett A 2008;372:631–6.
[22] Hayat T, Qasim M. Influence of thermal radiation and Joule heating on MHD flow of a Maxwell fluid in the presence of thermophoresis. Int J Heat Mass Transfer 2010;53:4780–8.
[23] Gireesha BJ, Mahanthesh B, Gorla RSR, Manjunatha PT. Thermal radiation and Hall effects on boundary layer flow past a non-isothermal stretching surface embedded in porous medium with non-uniform heat source/sink and fluid-particle suspension. Heat Mass Transfer 2015; 24 1–15. http://dx.doi.org/10.1007/s00231-015-1606-3.
[24] Pantokratoras A, Fang T. Sakiadis flow with nonlinear Rosseland thermal radiation. Phys Scr 2013;87:015703. (5 pages).

[25] Cortell R. Fluid flow and radiative nonlinear heat transfer over a stretching sheet. J King Saud Univ Sci 2014;26:161–7.
[26] Mushtaq A, Mustafa M, Hayat T, Alsaedi A. Effects of thermal radiation on the stagnation-point flow of upper-converted Maxwell fluid over a stretching sheet. J Aerosp Eng 2014;27: http://dx.doi.org/10.1061/(ASCE)AS.1943-5525.0000361.
[27] Mushtaq A, Mustafa M, Hayat T, Alsaedi A. Nonlinear radiative heat transfer in the flow of nanofluid due to solar energy: A numerical study. J Taiwan Inst Chem Eng 2014;45:1176–83.
[28] S.U.S. Choi, J.A. Eastman, Enhancing thermal conductivity of fluids with nanoparticles. The Proceedings of the ASME International Mechanical Engineering Congress and Exposition. ASME, San Francisco, USA, FED 231/MD 1995;66:99–105,
[29] Abbasi, F.M., Shehzad, S.A., Hayat, T., Alsaedi, A and Mustafa A. Obid. Influence of heat and mass flux conditions in hydromagnetic flow of Jeffrey nanofluid. AIP Advances, 2015; 5, 037111 doi: 10.1063/1.4914549.
[30] Bilal Ashraf, M., Hayat, T., Alsaedi, A and Shehzad, S.A. Convective heat and mass transfer in MHD mixed convection flow of Jeffrey nanofluid over a radially stretching surface with thermal radiation. J. Cent. South Univ 2015; 22:1114−1123.
[31] Krishnamurthy, M.R., Prasannakumara, B.C., Gireesha, B.J and Rama Subba Reddy Gorla. “Effect of chemical reaction on MHD boundary layer flow and melting heat transfer of Williamson nanofluid in porous medium”. Journal of Engineering Science and Technology 2015; http://dx.doi.org/10.1016/j.jestch.2015.06.010.
[32] Hayat, T., Muhammad, T., Shehzad, S and Alsaedi, A. "Three-Dimensional Flow of Jeffrey Nanofluid with a New Mass Flux Condition." J. Aerosp. Eng 2015; 0.1061/(ASCE)AS.1943-5525.0000549 , 04015054.
[33] Shehzad, S.A., Hayat, T and Alsaedi, A. “MHD flow of Jeffrey nanofluid with convective boundary conditions”. Journal of the Brazilian Society of Mechanical Sciences and Engineering, 2015; 73 (3): 873-883.
[34] Shehzad, S.A., Abdullah, Z., Alsaedi, A., Abbasi, F.M and Hayat, T. “Thermally radiative three-dimensional flow of Jeffrey nanofluid with internal heat generation and magnetic field”. Journal of Magnetism and Magnetic Materials 2015; 397:108–114.
[35] Nemat Dalira, Mohammad Dehsara and Salman Nourazar, S. “Entropy analysis for magnetohydrodynamic flow and heat transfer of a Jeffrey nanofluid over a stretching sheet”. Energy, 2015;79: 351–362.
[36] Prasannakumara B.C., Gireesha B.J., Rama Subba Reddy Gorla and Krishnamurthy M.R, Effects of chemical reaction and nonlinear thermal radiation on Williamson nanofluid slip flow over a stretching sheet embedded in a porous medium, Accepted in Journal of Aerospace Engineering 2016;:http://dx.doi.org/10.1061/(ASCE)AS.1943-5525.0000578.

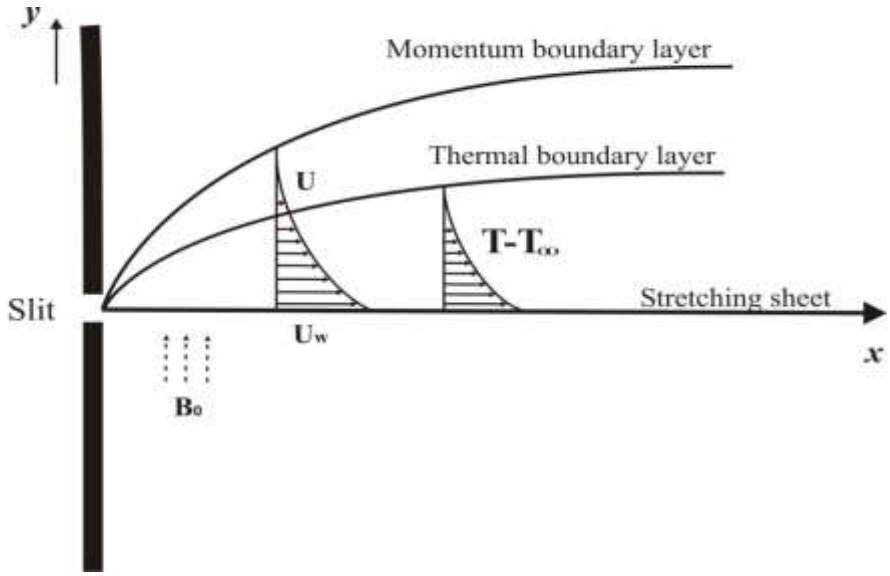

Fig. 1: Physical model and coordinate system.

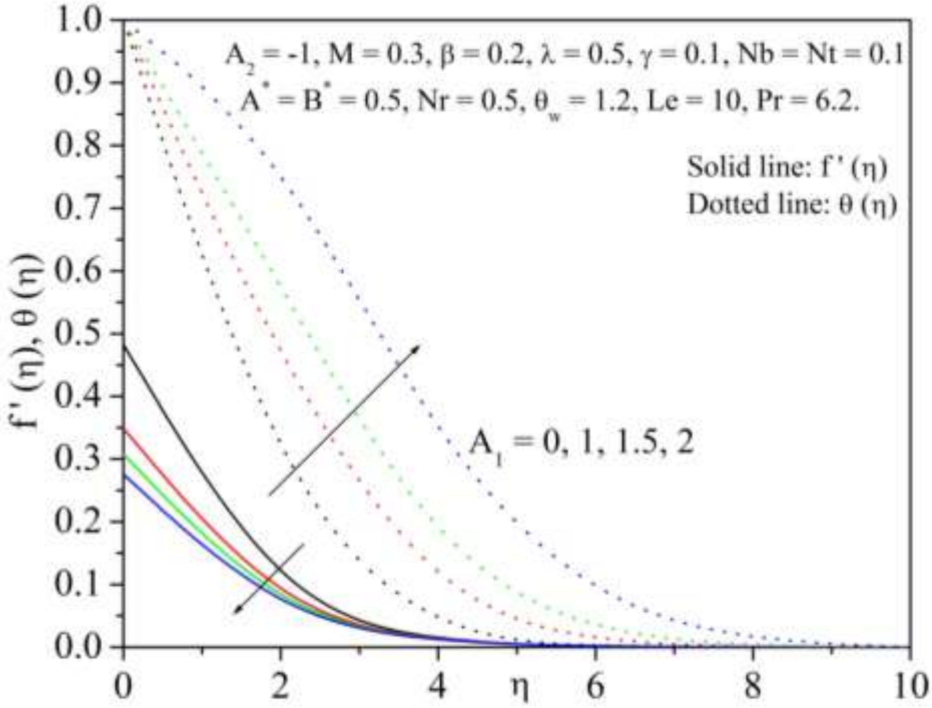

Fig. 2: Velocity and temperature profile for various values of A_1.

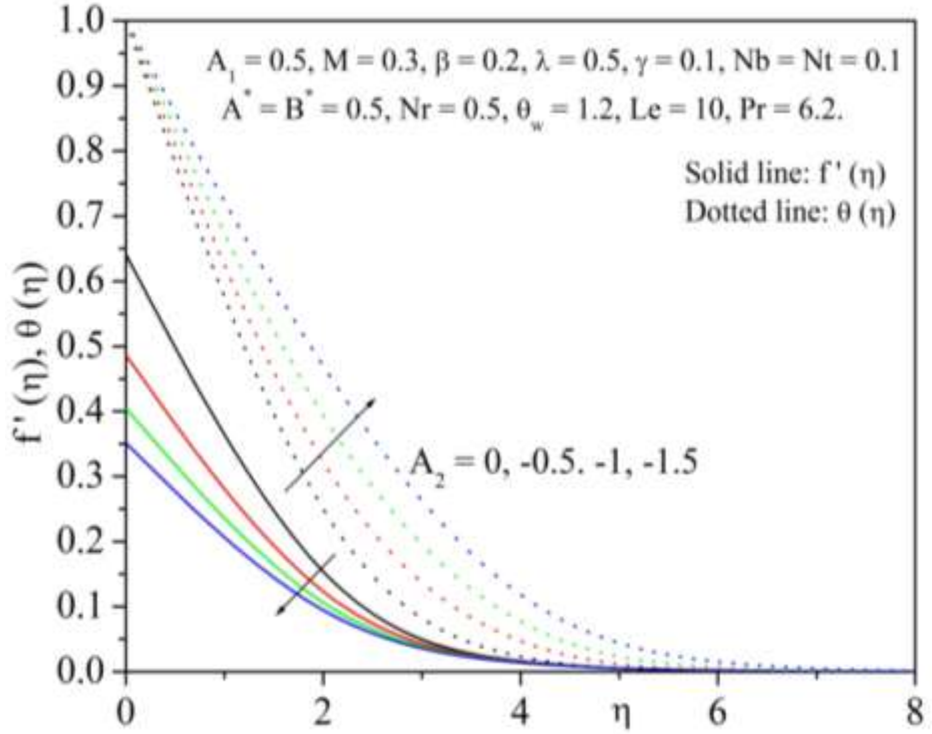

Fig. 3: Velocity and temperature profile for various values of A_2.

ISSN: 2277-9655
Impact Factor: 4.116
CODEN: IJESS7

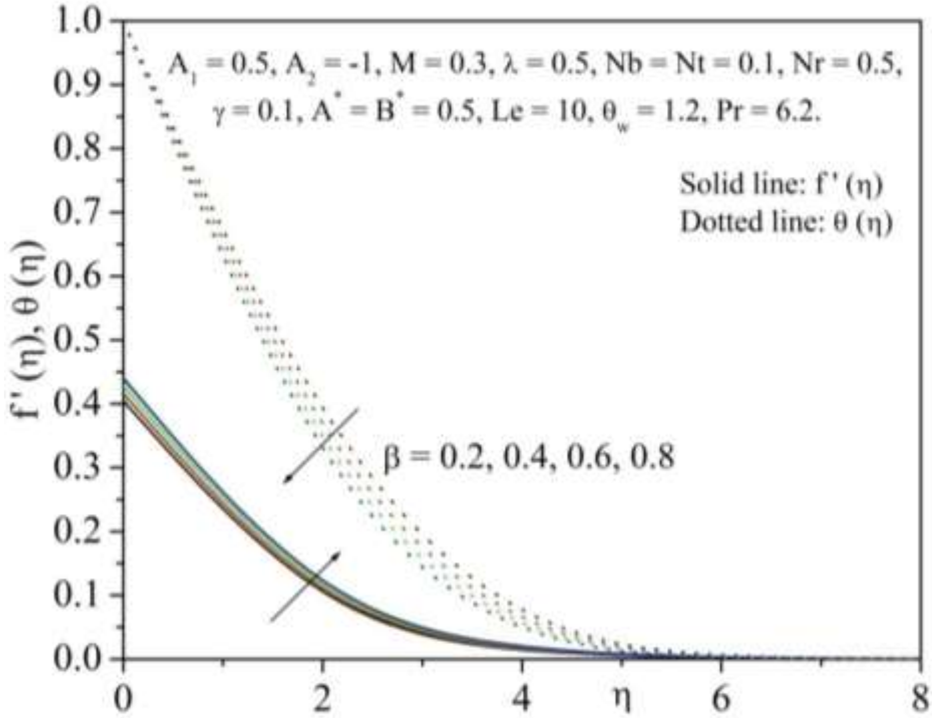

Fig. 4: Velocity and temperature profile for various values of β.

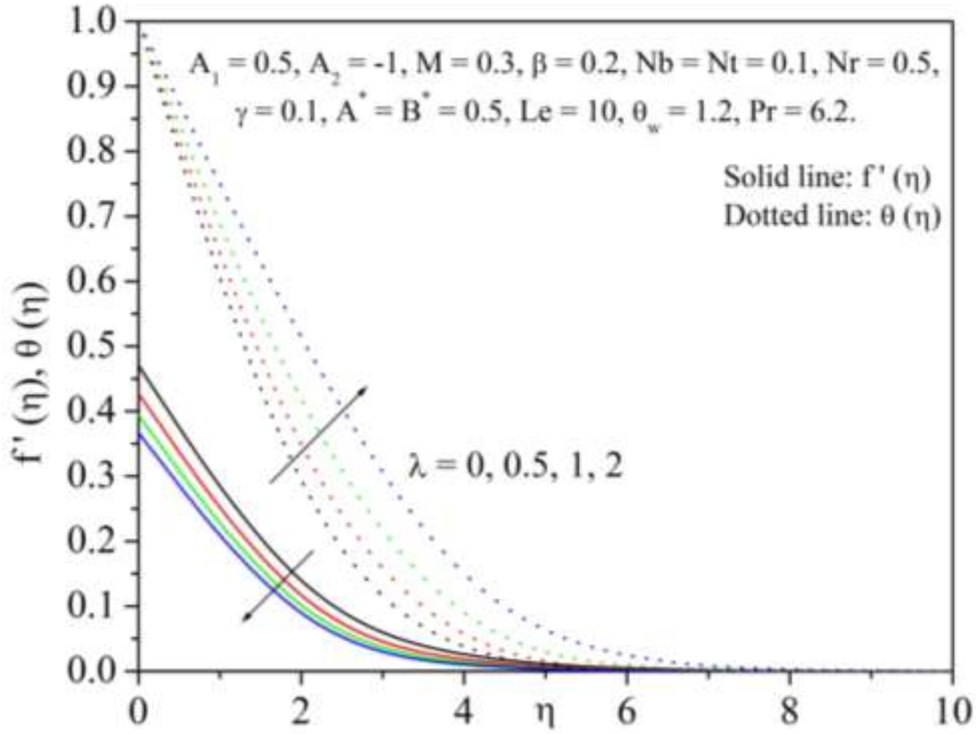

Fig. 5: Velocity and temperature profile for various values of λ.

ISSN: 2277-9655
Impact Factor: 4.116
CODEN: IJESS7

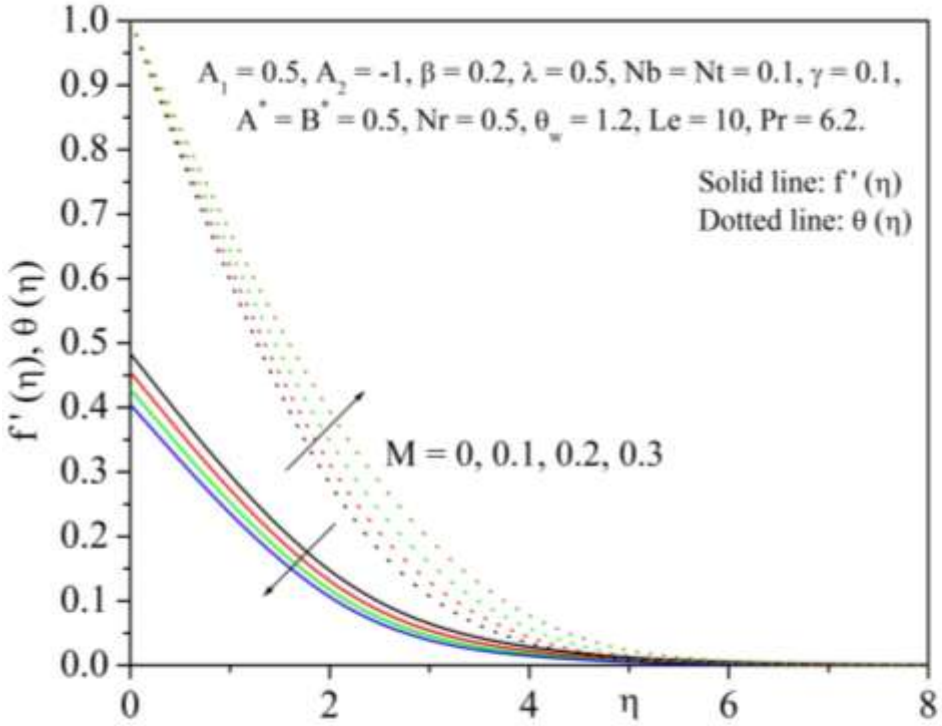

Fig. 6: Velocity and temperature profile for various values of M.

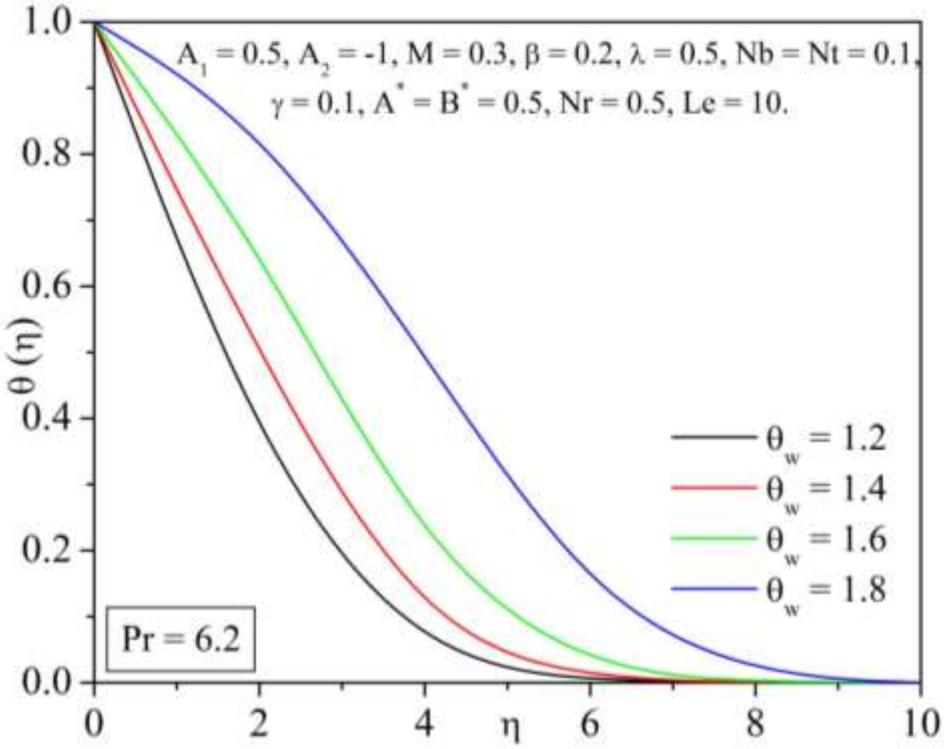

Fig. 7: Temperature profile for various values of θ_w when $Pr = 6.2$.

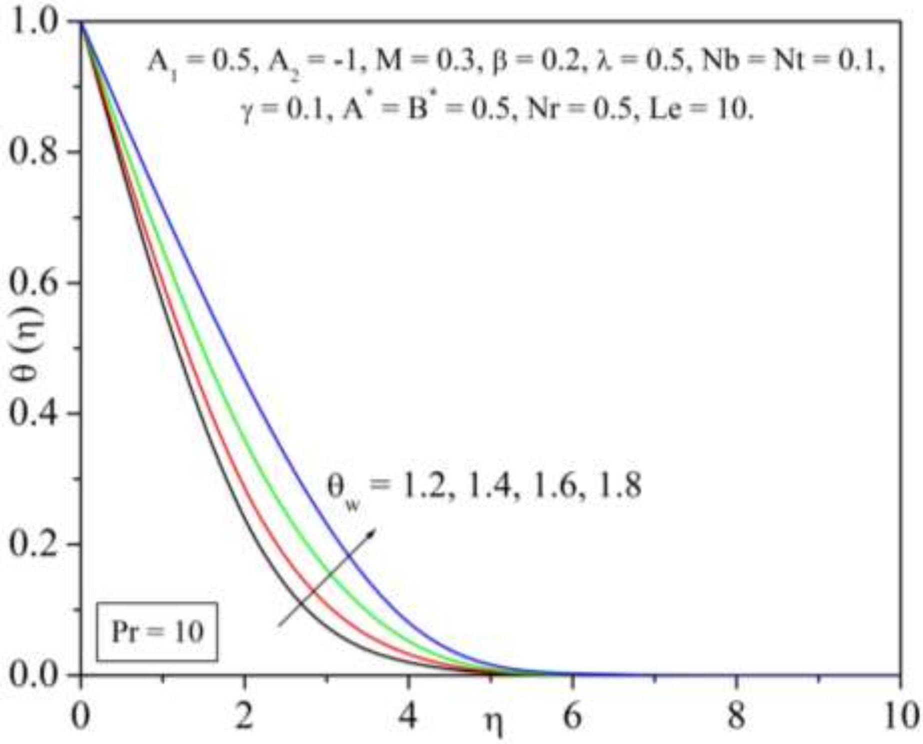

Fig. 8: Temperature profile for various values of θ_w when $Pr = 10$.

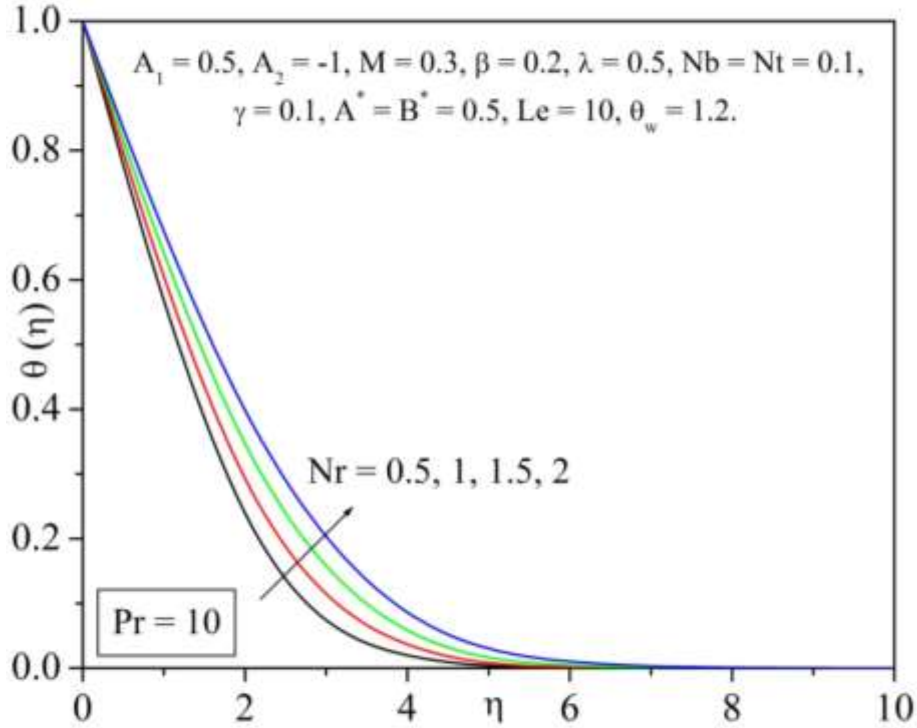

Fig. 9: Temperature profile for various values of Nr.

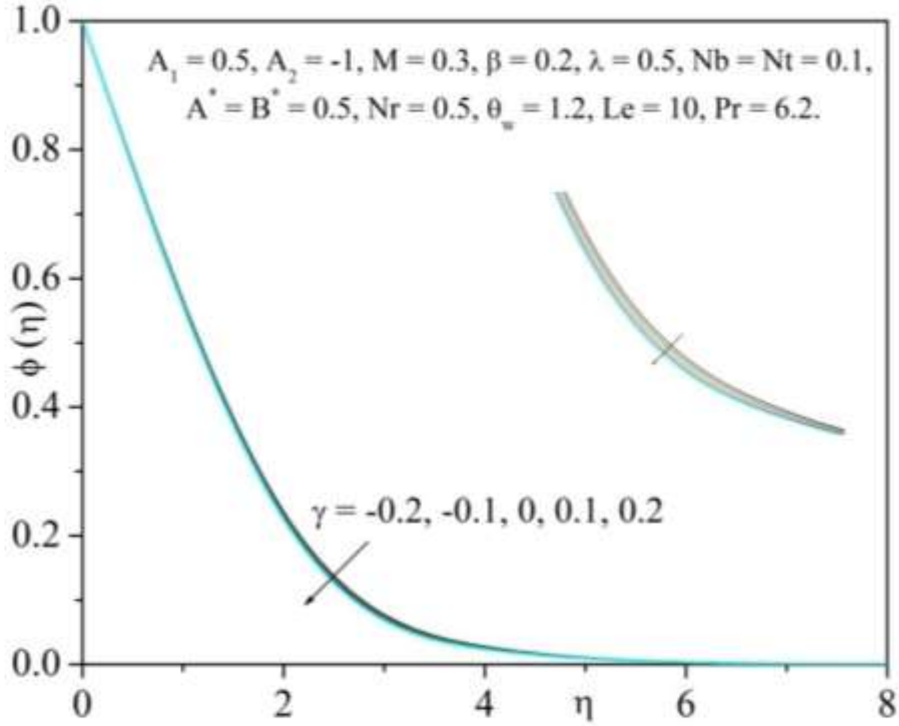

Fig. 10: Nanoparticle concentration profile for various values of γ.

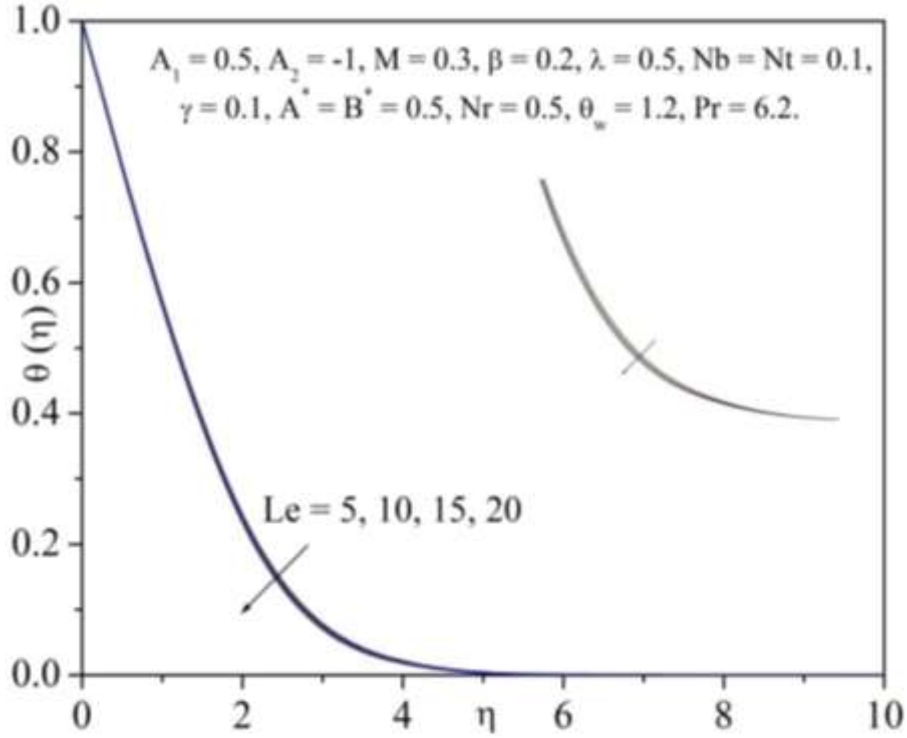

Fig. 11: Temperature profile for various values of Le.

ISSN: 2277-9655
Impact Factor: 4.116
CODEN: IJESS7

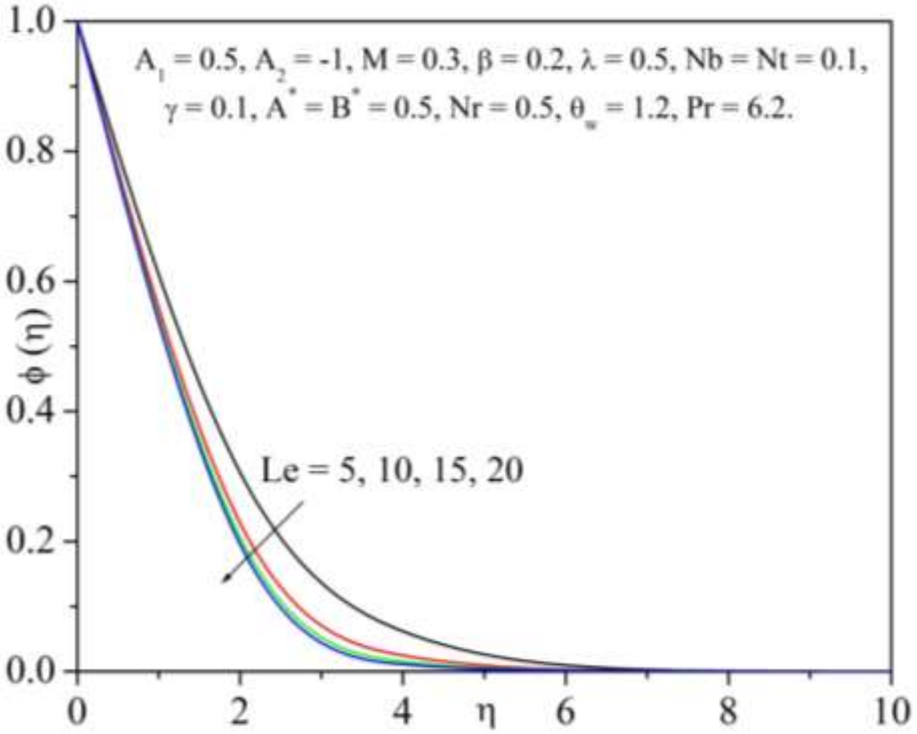

Fig. 12: Nanoparticle concentration profile for various values of Le.

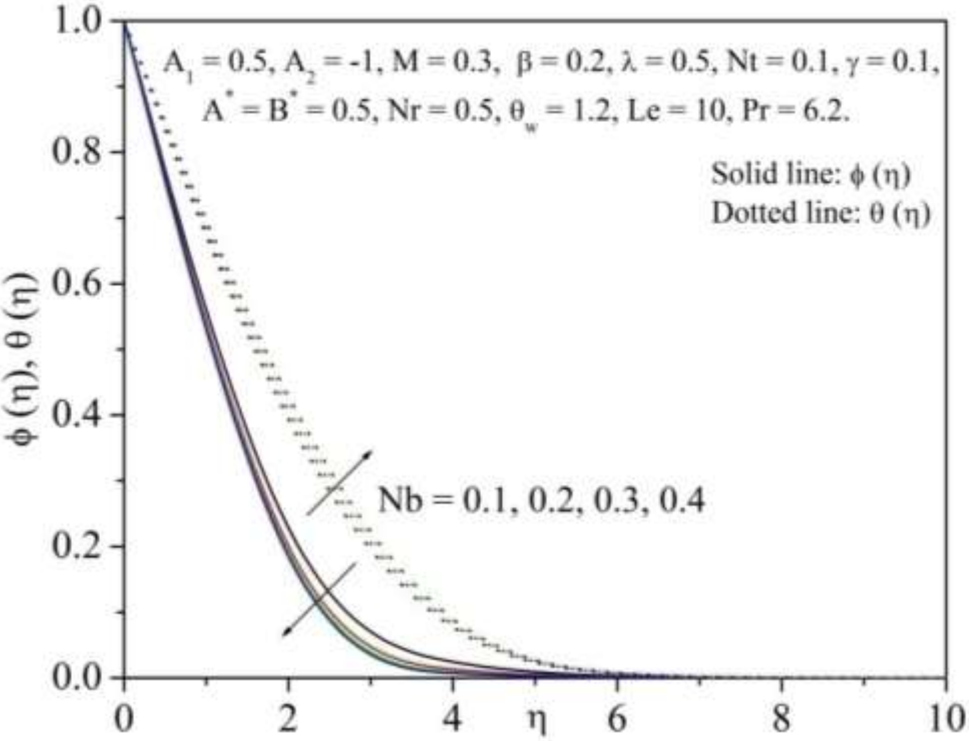

Fig. 13: Temperature and Nanoparticle concentration profile for various values of Nb.

ISSN: 2277-9655
Impact Factor: 4.116
CODEN: IJESS7

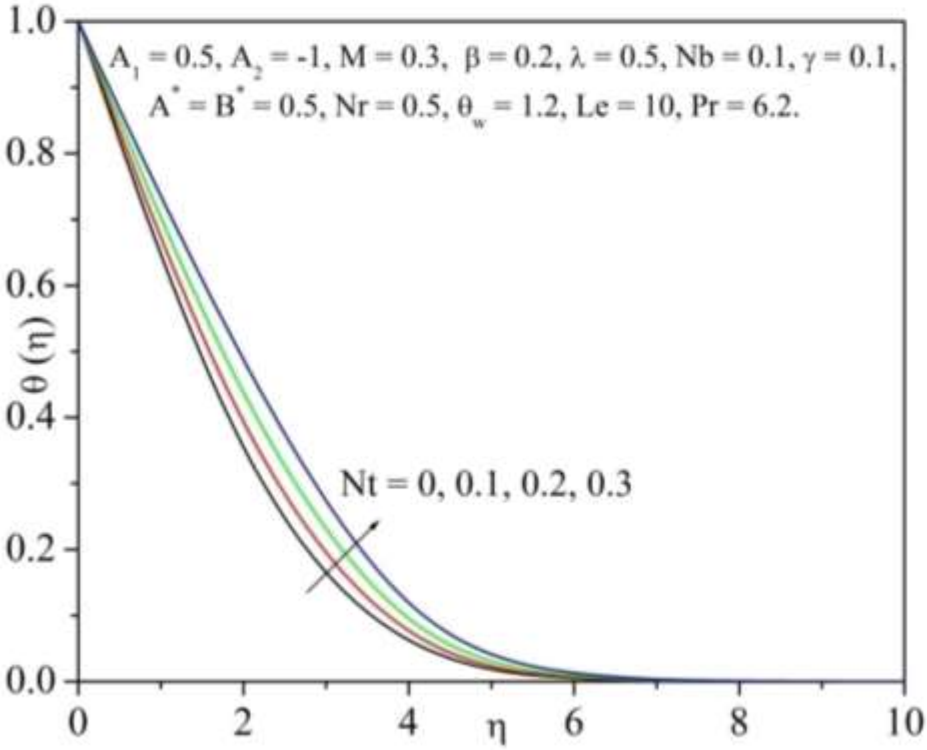

Fig. 14: Temperature profile for various values of Nt.

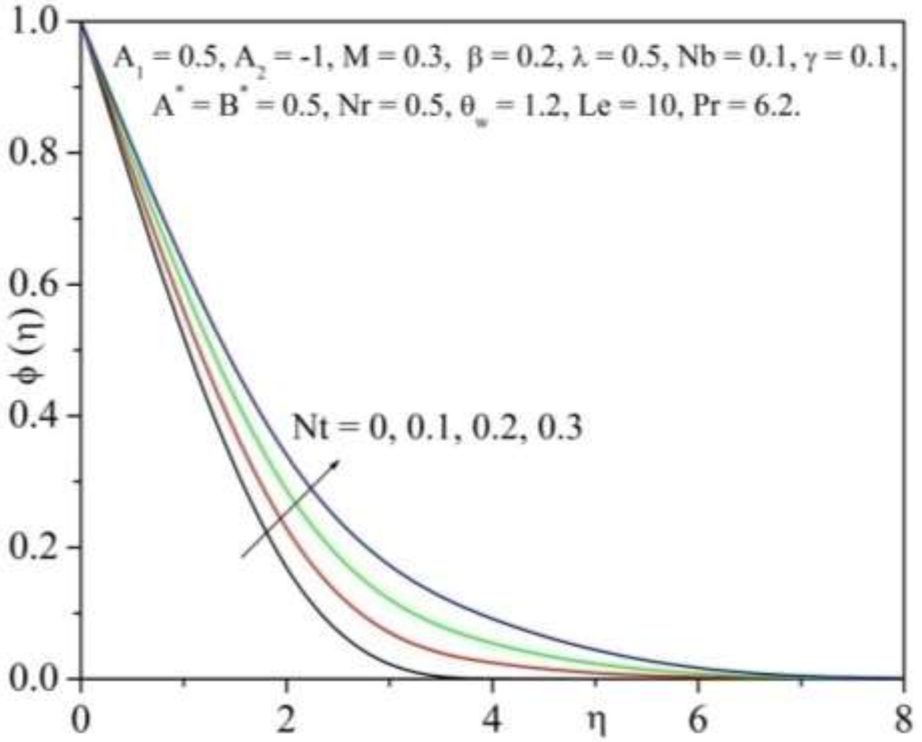

Fig. 15: Nanoparticle concentration profile for various values of Nt.

ISSN: 2277-9655
Impact Factor: 4.116
CODEN: IJESS7

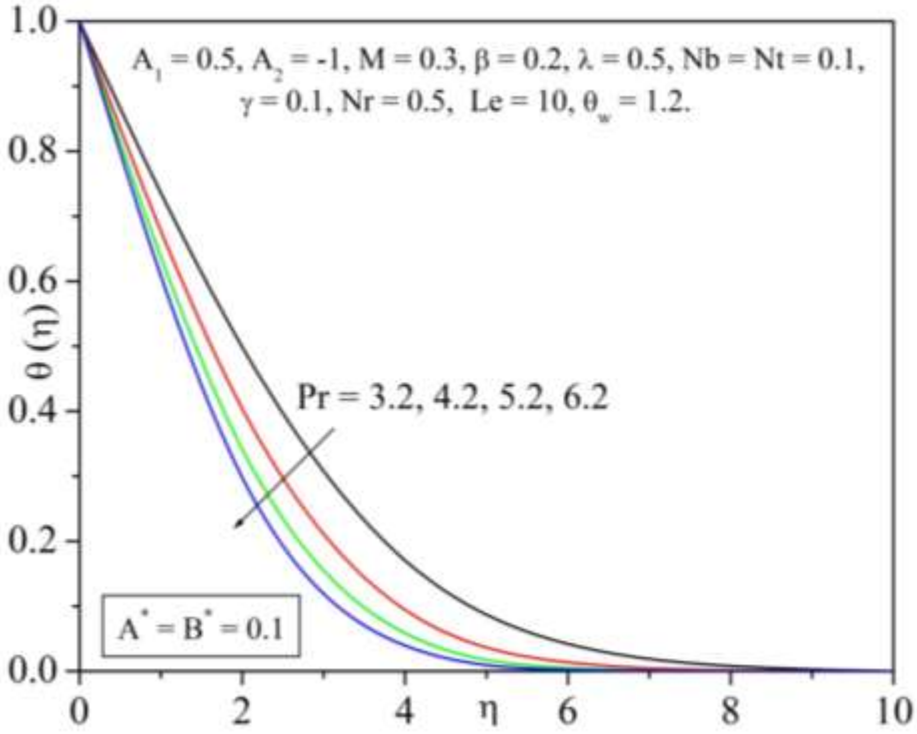

Fig. 16: Temperature profile for various values of Pr.

Table1.Comparison table for $-\theta'(0)$(viscous case)with $\beta = \lambda = A_1 = A_2 = Nr = \gamma = 0, Nb = Nt = 10^{-6}$.

Pr	Nadeem and Hussain(HAM method)(2013)	Gorla and Sidawi(1994)	Goyal and Bhargava (FEM Method)(2014)	Wang (1989)	Present (RKF45 Method)
0.2	0.169	0.1691	0.1691	0.1691	0.170259788
0.7	0.454	0.5349	0.4539	0.4539	0.454447258
2	0.911	0.9114	0.9113	0.9114	0.911352755
7		1.8905	1.8954	1.8954	1.895400395
20		3.3539	3.3539	3.3539	3.353901838

Table 2: Values of Skin friction coefficient and Nusselt number for different values of the parameters when $Pr = 6.2, \theta_w = 1.2, Nr = 0.5$.

A_1	A_2	β	λ	M	$-\sqrt{Re}Cf_x$	$-\frac{Nu_x}{\sqrt{Re_x}}$
0					0.3650	0.4217
1					0.2380	0.1771
1.5					0.2020	0.0403
	0				0.5400	0.6069
	-0.5				0.3690	0.4266
	-1				0.2880	0.2973
		0.2			0.2880	0.2973
		0.4			0.3110	0.3360
		0.6			0.3350	0.3702
			0		0.4320	0.4736

ISSN: 2277-9655
Impact Factor: 4.116
CODEN: IJESS7

			0.3		0.3330	0.3687
			0.6		0.2700	0.2598
				0	0.2880	0.5004
				0.1	0.2890	0.4375
				0.2	0.2890	0.3708

Table 3: Values of Nusselt and Sherwood number for different values of the parameters when $\boldsymbol{A_1 = 0.5, A_2 = -1, \beta = 0.2, \lambda = 0.5, M = 0.3}$.

Nr	θ_w	Nb	Nt	γ	Le	Pr	$-\frac{Sh_x}{\sqrt{Re_x}}$	$-\frac{Nu_x}{\sqrt{Re_x}}$
0.5							1.4502	0.2973
1							1.4521	0.3246
1.5							1.4558	0.2691
	1.2						1.4521	0.2973
	1.4						1.4520	0.2642
	1.6						1.4510	0.1956
		0.1					1.4540	0.2973
		0.2					1.4521	0.2066
		0.3					1.4520	0.1350
			0				1.4250	0.3916
			0.1				1.4521	0.2973
			0.2				1.5174	0.2113
				-0.2			1.3169	0.2971
				-0.1			1.3639	0.2970
				0			1.4089	0.2972
				0.1			1.4521	0.2973
				0.2			1.4936	0.2975
					5		0.9829	0.3001
					10		1.4521	0.3000
					20		2.1209	0.2973
						4.2	1.3598	0.5251
						5.2	1.3471	0.6073
						6.2	1.3380	0.6705